10 DFT-based Green Function Approach for Impurity Calculations

Rudolf Zeller
Institute for Advanced Simulation
Forschungszentrum Jülich GmbH

Contents

E. Pavarini, E. Koch, F. Anders, and M. Jarrell
Correlated Electrons: From Models to Materials
Modeling and Simulation Vol. 2
Forschungszentrum Jülich, 2012, ISBN 978-3-89336-796-2
http://www.cond-mat.de/events/correl12

1 Introduction

If one wants to apply density functional theory (DFT) to study the electronic structure of materials locally perturbed by defect atoms or more generally of disordered dilute and concentrated alloys, the standard approach is to use band structure methods developed for periodic systems. The defect atoms are periodically repeated so that a periodic crystal with a large unit cell (supercell) is obtained. The supercell must be large to minimize spurious interactions between the defect atoms in adjacent supercells. Supercells with a few hundred atoms can be treated routinely today and sophisticated corrections for some of the unwanted interactions have been developed. The situation was considerably different in the 1970s and 1980s when the computing power was orders of magnitude smaller than today. Then Green function methods were mandatory to investigate the electronic structure of defect atoms more efficiently. The advantage of Green function methods is that the potential must be determined self-consistently only in the region where it noticeably differs from the one of the unperturbed host crystal. As a consequence Green function methods correctly describe the embedding of the local environment of the defect atoms in the otherwise unperturbed surrounding perfect crystal. It is the aim of this chapter to give an introduction into the concept of Green function methods for studying locally perturbed crystals. For illustration of the concept and its advantages some key results will be presented. These results were mainly obtained by a Green function (GF) technique which is based on the Korringa-Kohn-Rostoker (KKR) band structure method [1, 2] and which was developed in Jülich over the last decades. This technique, the KKR-GF method, is particularly suited for metallic systems, but can be applied also for semiconductors and insulators.

2 Green function of the Kohn-Sham equation

The basic quantity in density functional theory [3, 4] is the electronic density. The density can be determined, if the Kohn-Sham single-particle equations

$$\left[-\nabla_{\mathbf{r}}^2 + v_{\text{eff}}(\mathbf{r})\right] \varphi_i(\mathbf{r}) = \epsilon_i \varphi_i(\mathbf{r}) \tag{1}$$

are solved.[1] The normalized Kohn-Sham wavefunctions $\varphi_i(\mathbf{r})$ can then be used to calculate the density by

$$n(\mathbf{r}) = 2 \sum_i |\varphi_i(\mathbf{r})|^2 \tag{2}$$

where for a system with N electrons the sum is over the $N/2$ orbitals with the lowest values of ϵ_i. The ϵ_i are the eigenvalues of the Hamiltonian $\mathcal{H} = -\nabla_{\mathbf{r}}^2 + v_{\text{eff}}(\mathbf{r})$. The factor two accounts for the assumed spin degeneracy. Alternatively to (2), the density can be calculated from the Green function of the Kohn-Sham system. This Green function is defined as the solution of

$$\left[-\nabla_{\mathbf{r}}^2 + v_{\text{eff}}(\mathbf{r}) - \epsilon\right] G(\mathbf{r}, \mathbf{r}'; \epsilon) = -\delta(\mathbf{r} - \mathbf{r}') \, . \tag{3}$$

[1] To simplify the notation, Rydberg atomic units $\hbar^2/2m = 1$ are used throughout this chapter and usually the equations are given only for non-spin-polarized systems. The generalization to spin-polarized (magnetic) systems is straightforward.

Here the boundary condition $G(\mathbf{r},\mathbf{r}';\epsilon) \to 0$ for $|\mathbf{r}-\mathbf{r}'| \to \infty$ is assumed and the symbol ϵ denotes a continuous complex variable in contrast to the real discrete variables ϵ_i. The result for the density is

$$n(\mathbf{r}) = -\frac{2}{\pi}\mathrm{Im}\int_{-\infty}^{E_F} G(\mathbf{r},\mathbf{r};\epsilon)\mathrm{d}\epsilon \tag{4}$$

where the integral is understood as an integral in the complex ϵ plane on a contour infinitesimally above the real ϵ axis. The Fermi level E_F is obtained by the condition that the density $n(\mathbf{r})$ integrated over all space gives the correct number of electrons. For instance, in neutral systems, this number is determined by the sum of the nuclear charges. The result (4) can be derived as follows. In operator notation (3) can be written as

$$[\mathcal{H}-\epsilon]G = -I \tag{5}$$

where $\mathcal{H}$ is the Hamiltonian and I the unity operator. In terms of eigenvalues ϵ_i and eigenfunctions $\varphi_i(\mathbf{r})$ the Hamiltonian $\mathcal{H}$ can be expressed as

$$\mathcal{H} = \sum_i \epsilon_i \varphi_i(\mathbf{r})\varphi_i^\star(\mathbf{r}')\,. \tag{6}$$

This is true because the right hand of this equation acting on $\varphi_i(\mathbf{r})$ leads to $\epsilon_i\varphi_i(\mathbf{r})$ which is the required result for $\mathcal{H}\varphi_i(\mathbf{r})$. This follows from

$$\sum_j \epsilon_j\varphi_j(\mathbf{r})\int \mathrm{d}\mathbf{r}'\varphi_j^\star(\mathbf{r}')\varphi_i(\mathbf{r}') = \sum_j \epsilon_j\varphi_j(\mathbf{r})\delta_{ij} = \epsilon_i\varphi_i(\mathbf{r}) \tag{7}$$

where the orthonormality constraint $\int \mathrm{d}\mathbf{r}'\varphi_j^\star(\mathbf{r}')\varphi_i(\mathbf{r}') = \delta_{ij}$ for the eigenfunctions was used. By using that G is the inverse operator of $\epsilon - \mathcal{H}$ the so called spectral representation

$$G(\mathbf{r},\mathbf{r}';\epsilon) = \sum_i \frac{\varphi_i(\mathbf{r})\varphi_i^\star(\mathbf{r}')}{\epsilon-\epsilon_i} \tag{8}$$

for the Green function is obtained. If this representation is inserted in (4) and the identity

$$\lim_{y\to 0^+}\frac{1}{x+\mathrm{i}y} = \mathrm{P}\frac{1}{x} - \mathrm{i}\pi\delta(x) \tag{9}$$

is applied to evaluate the imaginary part of (8), a delta function $\delta(\epsilon-\epsilon_i)$ appears which then can be used to perform the integration in (4). The upper integration limit E_F restricts the sum to eigenfunctions with $\epsilon_i \le E_F$ and the equivalence of (2) and (4) is demonstrated.
Equation (8) shows that the Green function has poles on the real ϵ axis at discrete values ϵ_i. These values represent the discrete part of the eigenvalue spectrum. In general, also a continuous part of the eigenvalue spectrum is possible. For instance in free space, with $v_{\mathrm{eff}}(\mathbf{r}) = 0$, the eigenfunctions are plane waves $\mathrm{e}^{\mathrm{i}\mathbf{k}\mathbf{r}}$ with eigenvalues given by k^2. These eigenvalues continuously cover the non-negative part of the real ϵ axis. Then (8) must be generalized into

$$G(\mathbf{r},\mathbf{r}';\epsilon) = \sum_i \frac{\varphi_i(\mathbf{r})\varphi_i^\star(\mathbf{r}')}{\epsilon-\epsilon_i} + \int_{-\infty}^{\infty}\frac{\varphi(\mathbf{r};\epsilon')\varphi^\star(\mathbf{r}';\epsilon')}{\epsilon-\epsilon'}\mathrm{d}\epsilon' \tag{10}$$

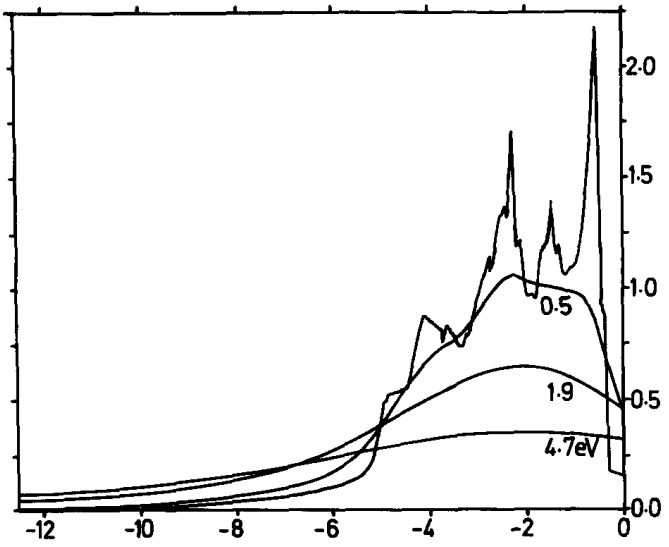

Fig. 1: *Density of states for Ni (here only for majority electrons) and the corresponding quantity along paths parallel to the real axis with distance 0.5, 1.8 and 4.7 eV. The picture is taken from Ref. [8]. It illustrates the increasing smoothness of the integrand with increasing distance from the real axis.*

where the integral is over the continuous part of the spectrum. In periodic crystals the continuous part of the spectrum is realized by bands, for instance by the valence and conduction bands in semiconductors. For the numerical evaluation of (4) it is important that the Green function is an analytical function[2] of ϵ except for the singularities on the real axis. This means that the integration (4) can be performed on a contour in the complex ϵ plane where the integrand is much smoother than just above the real axis as illustrated in Fig. 1. This procedure was suggested in a number of papers [6–9] and leads to considerable savings of computing time. Usually 30 to 40 points in the complex ϵ plane are enough for accurate evaluations of (4) provided that the points are chosen dense enough near E_F, where the contour necessarily approaches the real axis.
An important quantity, which is often used to provide an understanding of the electronic structure of materials in a single-particle picture, is the local density of states within in a volume V. It is defined as

$$n_V(\epsilon) = 2\sum_i \delta(\epsilon_i - \epsilon) \int_V \mathrm{d}\mathbf{r}\, |\varphi_i(\mathbf{r})|^2 \tag{11}$$

and gives the distribution of occupied and unoccupied electronic states within the volume V, for instance the local volume corresponding to one atom in the system. In terms of the Green function the local density of states is given by

$$n_V(\epsilon) = -\frac{2}{\pi} \operatorname{Im} \int_V \mathrm{d}\mathbf{r}\, G(\mathbf{r}, \mathbf{r}; \epsilon) \tag{12}$$

as can be verified by using the spectral representation (8). The total density of states is obtained if the integrals in (11) or (12) are done over all space.

[2]For an elementary introduction to classical Green functions and their analytical properties the textbook of Economou [5] is a good source.

3 Green function method for impurities

Historically the Green function method is attributed to Koster and Slater [10] who expanded the Green function in terms of Wannier functions. Because of the difficult construction of Wannier functions at that time the capabilities of this approach were rather limited. At the end of the 1970s Green function methods for the calculation of the electronic structure of impurities in solids received new attention. Inspired by the success of DFT calculations for periodic solids, several groups invested a considerable amount of work into the development of Green function methods for impurity calculations. They used a number of different techniques to calculate the the Green function of the periodic host crystal which is needed for the subsequent impurity calculations. The LCAO-GF method [11,12] was based on an expansion in linear combinations atomic orbitals, the LCGO-GF method [13] on an expansion in linear combination of Gaussian orbitals, the LMTO-GF method [14,15] on the linear muffin-tin orbital method and the KKR-GF method [16, 17] on the Korringa-Kohn-Rostoker band structure method.
In the beginning the Green functions were calculated mostly by using the spectral representation (8). This is easy for the imaginary part of the Green function because according to (9) the imaginary part of the denominator $\epsilon - \epsilon_i$ leads to a delta function so that only ϵ_i values contribute which are in the ϵ range for which the Green function is needed. From the imaginary part the real part was then obtained by the Kramers-Kronig relation

$$\mathrm{Re}\, G(\mathbf{r}, \mathbf{r}'; \epsilon) = -\frac{1}{\pi} P \int_{-\infty}^{\infty} \mathrm{d}\epsilon' \frac{1}{\epsilon - \epsilon'} \mathrm{Im}\, G(\mathbf{r}, \mathbf{r}'; \epsilon') \,. \tag{13}$$

Here in principle, the imaginary part is needed along the entire real ϵ axis. In practice, approximations were used, either the imaginary part in the integrand was neglected for higher ϵ values or it was replaced by an analytical approximation [18]. Another possibility is to use basis functions in a finite Hilbert space [15].
The problem that an infinite number of eigenstates contributes in (8) can be avoided if the host Green function is directly calculated by Brillouin zone integrations. This technique, which directly calculates the Green function for a given energy, is used in the KKR coherent potential approximation (KKR-CPA) [19, 20] and has been implemented also in the KKR-GF method. This procedure is perhaps most easily understood in terms of reference Green functions. Instead of using the defining differential equation (3) or the spectral representation (8), the Green function is calculated from the integral equation

$$G(\mathbf{r}, \mathbf{r}'; \epsilon) = G^r(\mathbf{r}, \mathbf{r}'; \epsilon) + \int \mathrm{d}\mathbf{r}'' G^r(\mathbf{r}, \mathbf{r}''; \epsilon) \Delta v(\mathbf{r}'') G(\mathbf{r}'', \mathbf{r}'; \epsilon) \,. \tag{14}$$

Here G^{r} is the Green function of a suitably chosen reference system with reference potential $v^{\mathrm{r}}(\mathbf{r})$ and $\Delta v(\mathbf{r}) = v_{\mathrm{eff}}(\mathbf{r}) - v^{\mathrm{r}}(\mathbf{r})$ is the perturbation of the potential given by the difference of the Kohn-Sham potential and the reference potential. The Green function G^{r} is determined by

$$\left[-\nabla^2_{\mathbf{r}} + v^{\mathrm{r}}(\mathbf{r}) - \epsilon\right] G^{\mathrm{r}}(\mathbf{r}, \mathbf{r}'; \epsilon) = -\delta(\mathbf{r} - \mathbf{r}') \,. \tag{15}$$

The calculation of Green functions by using reference systems is a powerful concept for the calculation of the electronic structure for systems with a complicated geometric structure. An

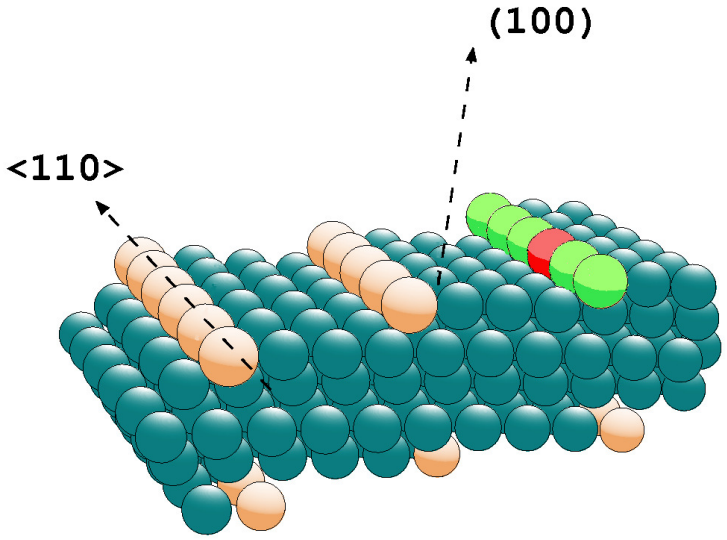

Fig. 2: *Illustration for the geometry of one impurity atom in an atomic chain which consists of other atoms than the otherwise periodically repeated chains at the step edges of a vicinal (711) surface of an fcc crystal.*

example for such a system, shown in Fig. 2, is a vicinal (711) surface of a face-centered-cubic crystal decorated with adatoms at step edges and within step edges. The Green function for this system can be constructed by the successive calculation of Green functions of simpler systems. i) Starting from free space the Green function for the bulk crystal is calculated treating the full bulk potential as perturbation using periodicity in three dimensions. ii) Several layers of the bulk crystal are removed, the removed potential is treated as perturbation using the two-dimensional surface periodicity. As a consequence of the fact the electrons cannot tunnel through several empty layers one obtains a slab which is decoupled from the rest of the bulk crystal. iii) Atomic chains are added at step edges. The potential perturbation is periodic in two dimension, but locally restricted to the vicinity of the step edges. iv) A chain of different atoms is inserted, only one-dimensional periodicity along the considered step edge is preserved, but the potential perturbation is confined to the vicinity of the considered chain. v) Finally, an impurity atom is inserted, periodicity is fully lost, but the potential perturbation is essentially confined to atoms in the vicinity of the impurity.

During this successive construction, periodicity can be used in the dimensions where it exists while in the remaining dimensions the potential perturbation is localized in the vicinity of the replaced atoms. In each successive step the integral equation must be solved only within a region of space where the potential differs non-negligibly from the one of the reference system. Once the Green function has been obtained for $\mathbf{r}$ and $\mathbf{r}'$ in this region, the Green function in all space can be obtained simply by multiplications and integrations. This represents an enormous advantage of Green function methods over supercell methods because the size of the region for which the integral equation must be solved is determined by the extent of the potential perturbation and not by the usually much larger extent of the perturbed wavefunctions or Green functions.

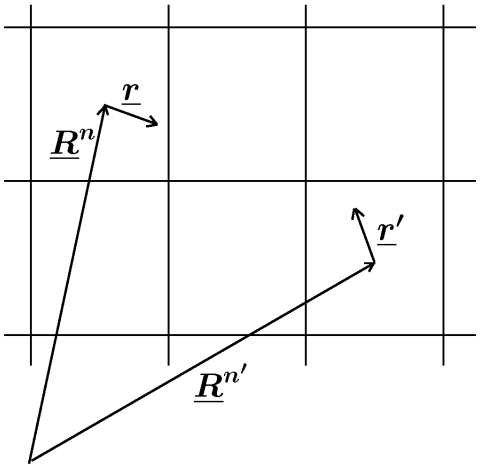

Fig. 3: *Partitioning of space and illustration for the definition of* $\mathbf{R}^n$ *and* $\mathbf{R}^{n'}$*, which define the positions of the cell centers, and* $\mathbf{r}$ *and* $\mathbf{r}'$*, which are vectors within the cells.*

An effective way to solve the integral equation (14) is provided by the KKR-GF method which does not rely on the determination of eigenvalues and eigenfunctions with their orthonormality constraints, but uses ideas of multiple-scattering theory. In this theory space is divided into non-overlapping regions, for instance cells around each atom, and the calculation of the Green function is broken up into two parts. First, *single-scattering* quantities, which depend only on the potential in a single cell, are determined. Second, the *multiple-scattering problem* is solved to obtain the correct combination of all single-scattering events.
The mathematical basis for the KKR-GF method is the fact that the Green function for free space, which is given by

$$G^0(\mathbf{r},\mathbf{r}';\epsilon) = -\frac{1}{4\pi}\frac{\exp(\mathrm{i}\sqrt{\epsilon}|\mathbf{r}-\mathbf{r}'|)}{|\mathbf{r}-\mathbf{r}'|}, \tag{16}$$

can be written in cell-centered coordinates as

$$G^0(\mathbf{r}+\mathbf{R}^n,\mathbf{r}'+\mathbf{R}^{n'};\epsilon) = \delta_{nn'}G^0(\mathbf{r},\mathbf{r}';\epsilon) + \sum_{LL'} J_L(\mathbf{r};\epsilon)G^{0,nn'}_{LL'}(\epsilon)J_{L'}(\mathbf{r}';\epsilon) \tag{17}$$

with analytically known Green function matrix elements $G^{0,nn'}_{LL'}(\epsilon)$ which do not depend on the radial coordinates r or r'. Here $\mathbf{R}^n$ and $\mathbf{R}^{n'}$ are the coordinates of the cell centers, usually the atomic positions, and $\mathbf{r}$ and $\mathbf{r}'$ are coordinates within the cells which originate at the cell centers. An illustration for these coordinates is given in Fig. 3. The functions

$$J_L(\mathbf{r};\epsilon) = j_l(r\sqrt{\epsilon})Y_{lm}(\hat{\mathbf{r}}) \tag{18}$$

are products of spherical harmonics Y_{lm} with spherical Bessel functions. Angular variables are denoted by $\hat{\mathbf{r}} = \mathbf{r}/r$ and radial variables by $r = |\mathbf{r}|$. The symbol L is used as compact notation for the angular momentum indices l and m and sums over L denote double sums over l and $|m| \leq l$.

If one proceeds as in [21], it is straightforward to show that the solution of (14) is given by

$$G(\mathbf{r}+\mathbf{R}^n,\mathbf{r}'+\mathbf{R}^{n'};\epsilon)=\delta_{nn'}G^n_{\rm s}(\mathbf{r},\mathbf{r}';\epsilon)+\sum_{LL'}R^n_L(\mathbf{r};\epsilon)G^{nn'}_{LL'}(\epsilon)R^{n'}_{L'}(\mathbf{r}';\epsilon)\;. \tag{19}$$

Here $G^n_{\rm s}$ is the single-site Green function for cell n which satisfies the integral equation

$$G^n_{\rm s}(\mathbf{r},\mathbf{r}';\epsilon)=G^{\rm r}(\mathbf{r},\mathbf{r}';\epsilon)+\int_n {\rm d}\mathbf{r}''G^{\rm r}(\mathbf{r},\mathbf{r}'';\epsilon)\Delta v^n(\mathbf{r}'')G^n_{\rm s}(\mathbf{r}'',\mathbf{r}';\epsilon) \tag{20}$$

and R^n_L are the single-site solutions which satisfy the integral equations

$$R^n_L(\mathbf{r};\epsilon)=J_L(\mathbf{r};\epsilon)+\int_n {\rm d}\mathbf{r}'G^{\rm r}(\mathbf{r},\mathbf{r}';\epsilon)\Delta v^n(\mathbf{r}')R^n_L(\mathbf{r}';\epsilon)\;. \tag{21}$$

In (20-21) the integration is only over the volume of cell n and $\Delta v^n(\mathbf{r})=\Delta v(\mathbf{r}+\mathbf{R}^n)$ is the potential perturbation in this cell n. The Green function matrix elements $G^{nn'}_{LL'}$ used in (19) satisfy the matrix equation

$$G^{nn'}_{LL'}(\epsilon)=G^{r,nn'}_{LL'}(\epsilon)+\sum_{n''}\sum_{L''L'''}G^{r,nn''}_{LL''}(\epsilon)\Delta t^{n''}_{L''L'''}(\epsilon)G^{n''n'}_{L'''L'}(\epsilon) \tag{22}$$

which computationally represents a linear algebra problem. The difference Δt^n of the so-called single-site t matrices is given by

$$\Delta t^n_{LL'}(\epsilon)=\int_n {\rm d}\mathbf{r}\;J_L(\mathbf{r};\epsilon)\Delta v^n(\mathbf{r})R^n_{L'}(\mathbf{r};\epsilon)\;. \tag{23}$$

Together (19-23) provide a computationally convenient solution of the integral equation (14) without the need to determine eigenvalues and eigenfunctions. The only real approximation which must be made is the truncation of the infinite sums over L to a finite number of terms. This determines the angular momentum cutoff $l_{\rm max}$ used in the KKR-GF method. Usually $l_{\rm max}=3$ or $l_{\rm max}=4$ is sufficient for accurate results.

If the density of states integrated over all space is needed, for instance for the total energy calculations, it is important that the integration in (12) can be performed analytically if the volume V extends over all space. This is the essence of Lloyd's formula [22] which gives the difference of the integrated density of states

$$\Delta N(\epsilon)=\int^{\epsilon}{\rm d}\epsilon'\Delta n(\epsilon') \tag{24}$$

of the perturbed and unperturbed systems by logarithms of determinants. The formula can be written as

$$\Delta N(\epsilon)=\frac{1}{\pi}{\rm Im}\sum_n \Delta\ln\det|\alpha^n_{LL'}(\epsilon)|-\frac{1}{\pi}{\rm Im}\ln\det|\delta^{nn'}_{LL'}-\sum_{L'}G^{{\rm r},nn'}_{LL'}(\epsilon)\Delta t^{n'}_{L'L}(\epsilon)| \tag{25}$$

which is the KKR equivalent of the operator identity (61) derived in the appendix. The matrix α in (25) is defined by [23]

$$\alpha^n_{LL'}(\epsilon)=\delta_{LL'}+\int_n d\mathbf{r}H_L(\mathbf{r};\epsilon)v^n(\mathbf{r})R^n_{L'}(\mathbf{r};\epsilon) \tag{26}$$

for the potential $v^n(\mathbf{r})$ and analogously for the reference potential, where the functions

$$H_L(\mathbf{r};\epsilon)=h^{(1)}_l(r\sqrt{\epsilon})Y_{lm}(\hat{\mathbf{r}}) \tag{27}$$

are products of spherical harmonics with spherical Hankel functions of the first kind.

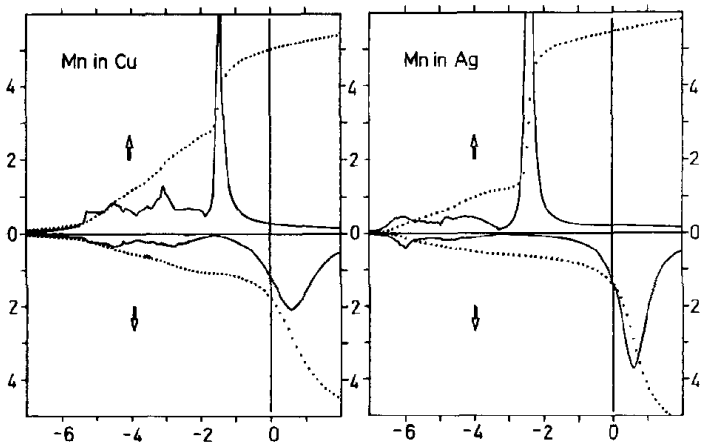

Fig. 4: *Local density of states (within the impurity cell) for Mn impurities in Cu and Ag as function of energy (in eV) relative to the Fermi level. The minority spin density of states is plotted downwards so that it does not overlap with the majority one. The dotted curves show the integrated density of states. The picture is taken from Ref. [25].*

3.1 Density of states

Although the single-particle eigenvalues ϵ_i and the density of states $n(\epsilon)$ calculated in density functional theory are only formal mathematical quantities, they often agree qualitatively with experiment and even more often they are used to provide a single-particle understanding of the chemical and physical mechanisms which lead to the observed behaviour of materials. Among the first systems studied by the KKR-GF method were $3d$ transition metal impurity atoms in noble metals which are the classical systems considered by Anderson in his famous paper on the Anderson impurity model [24].

In Fig. 4 the local density of states calculated with the local density approximation (LDA) of DFT is shown for Mn impurities in Cu and Ag. The differences for the two spin directions are caused by the fact that transition metal atoms of the Fe series can gain magnetic exchange energy by spin alignment. Anderson has discussed this behaviour in terms of Lorentzian type virtual bound states. Fig. 4 shows that these virtual bound states are reproduced in LDA-DFT calculations. In particular, the minority density of states shows almost Lorentzian type features with peak positions just above the Fermi level. However, also distortions from the Lorentzian form are clearly visible. They are caused by band structure effects arising from hybridization of the $3d$-states of the impurity atoms with the host d-states. Interestingly, in 1980 when Ref. [25] was published, it was seriously doubted that the observed splitting of the peak positions was the correct density functional answer, because conflicting results with much smaller splitting existed [26]. One criticism was that the observed spin splitting could be an artifact of the fact that only a potential perturbation in the impurity cell was used. Later calculations [27], where potential perturbations were also used in neighboring cells, confirmed the results shown in Fig. 4. Moreover, measurements [28,29] with various electron-spectroscopy techniques showed similar spin splittings as calculated. Fully quantitative agreement between calculations and experiment, of course, cannot be expected because states calculated with LDA are not to be identified as measurable quantities.

3.2 Defect formation energies

An important problem in the study of defects is the calculation of total energy differences which are the basic quantities necessary for understanding the microscopic origin of the formation of alloys and many other physical processes such as diffusion, short-range ordering, segregation. This is particularly true for vacancy formation and migration energies, which are difficult to measure, but important quantities to understand the thermodynamic and kinetic behaviour of metals and semiconductors. In supercell methods these numbers are difficult to calculate as expressed, for instance, in the following sentences taken from Puska *et al.* [30], who used supercells with up to 216 atoms. These authors write in the introduction *The vacancy in Si can be considered as the simplest example of a point defect in a semiconductor lattice* and in the conclusions *The convergence of the results is shown to be very slow* and *If the supercell is not large enough the long-range ionic relaxation pattern, especially in the [110] zigzag direction, may not be properly described*. Since then the vacancy in Si has been reinvestigated several times by supercell calculations, where due to the ever increasing computer power the supercell size has gradually increased. However, the convergence problem remains as stated in one of the most recent articles by Corsetti and Mostofi [31]. These authors who used supercells with up to 1000 atoms write in the conclusions *Our calculations confirm the slow finite size convergence of defect formation energies and transition levels, ...* They also argue that future increase of supercell sizes can reduce the spurious interactions between the vacancies in different cells, but that then another problem must be considered seriously. The problem is that total energy differences due to defect atoms are not calculated directly, but are obtained by numerical subtraction of supercell energies with and without defect. With increasing supercell size the numbers to be subtracted become larger which puts heavy demands on the numerical precision.

In contrast to supercell methods, Green function calculations are not plagued by these problems. The formation energy is calculated directly, not by energy differences, spurious interactions do not exist, and the region in space where the self-consistent calculations must be done is determined by the range of the potential perturbation and not by the usually much larger range of wavefunctions or Green function perturbations. Actually, the Si vacancy was considered as one of the earliest systems in Green function impurity calculations [11, 12]. At that time, however, it was not possible to calculate accurate total energies. Green function methods using basis sets suffered from insufficiently accurate basis functions and the KKR-GF method from the spherical approximation for the potential used in each cell. Only at the beginning of the 1990s accurate total energy calculations became possible, both due to the increased computing power and even more so because of the development of advanced numerical techniques. Results for some vacancy formation energies calculated by the KKR-GF method [32] are shown in Table 1. Compared to the original publication [33] the values for Cu and Ni contain corrections of about -0.04 and -0.08 eV which are energy gains obtained if the atoms relax to the correct equilibrium positions.

For the calculation of defect formation energies it is very important that Lloyd's formula is used to obtain the single-particle contribution. Within density functional theory the total energy con-

Table 1: *Calculated and experimental values for the vacancy formation energy of selected transition metals (in eV). The calculations for Cu and Ni include the effect of lattice relaxations.*

	Cu	Ag	Ni	Pd
Theory	1.37	1.20	1.68	1.57
Experiment	1.28	1.11	1.79, 1.63	1.85, 1.54

Table 2: *Solution energy (in eV) for a V impurity in Cu calculated using potential perturbations in the vanadium cell and in different numbers of shells of surrounding Cu neighbors.*

shells	0	1	2	3	4
cells	1	13	19	43	55
E_{Lloyd}	1.44	0.73	0.73	0.73	0.73
E_{local}	1.60	1.93	1.38	0.75	0.52

sists of a sum of the kinetic energy $T[n(\mathbf{r})]$, the electrostatic Hartree energy and the exchange correlation energy. The kinetic energy is usually evaluated as

$$T[n(\mathbf{r})] = \sum_i \epsilon_i - \int \mathrm{d}\mathbf{r}\, n(\mathbf{r}) v_{\mathrm{eff}}(\mathbf{r}) = \int^{E_F} \mathrm{d}\epsilon\, \epsilon\, n(\epsilon) - \int \mathrm{d}\mathbf{r}\, n(\mathbf{r}) v_{\mathrm{eff}}(\mathbf{r}) \tag{28}$$
$$= E_F N(E_F) - \int^{E_F} \mathrm{d}\epsilon\, N(\epsilon) - \int \mathrm{d}\mathbf{r}\, n(\mathbf{r}) v_{\mathrm{eff}}(\mathbf{r})$$

by using the single-particle energies ϵ_i, where the last result is obtained from integration by parts over ϵ. If the density of states $n(\epsilon)$ or the integrated density of states $N(\epsilon)$ is calculated from the Green function by (11) and (24), an explicit summation over all cells of the infinite crystal is required. This problem is avoided if Lloyd's formula (25) is used which already contains the integration over all space.

The different behaviour of the shell convergence of energies calculated with and without Lloyd's formula is illustrated in Table 2 where results for the solution energy for a vanadium impurity in copper are shown. While the use of Lloyd's formula leads to a converged result already for 13 cells, the use of (11) with summation over cells only gives poor results. This behaviour reflects the fact that wavefunction or Green function perturbations are much longer ranged than the potential perturbation. Density changes, which contribute, for instance, in the last term of (28) and in other parts of the energy functional, exist outside of the perturbed potential region, but these changes are unimportant because of the variational properties of the energy functional.

3.3 Forces and lattice relaxations

Substitutional impurities, in general, have a different size than the host atoms. This causes displacements of the neighboring atoms away from their ideal positions which they occupy in the unperturbed host crystal. In metals, because of the high coordination number, the displacements

are rather small and can be neglected in the calculations of many physical properties. However, sometimes the displacements have significant effects and their size and direction should be calculated. In electronic structure methods displacements are calculated usually from the condition that the forces on the atoms should vanish and the forces are determined usually by the Hellmann-Feynman theorem

$$\mathbf{F}^n = -\frac{\partial E}{\partial \mathbf{R}^n}\bigg|_{n(\mathbf{r};\mathbf{R^n})} - \int \mathrm{d}\mathbf{r}\, \frac{\delta E}{\delta n(\mathbf{r})} \frac{\partial n(\mathbf{r};\mathbf{R}^n)}{\partial \mathbf{R}^n} \tag{29}$$

which means that the force $\mathbf{F}^n$ on atom n is determined by the derivative of the total energy E with respect to the coordinate $\mathbf{R}^n$ of atom n. Here the first term, evaluated at constant density $n(\mathbf{r};\mathbf{R}^n)$, is the Hellmann-Feynman (HF) force and the second term is necessary if approximations are made in the solution of the Kohn-Sham equations. The second term vanishes in an exact treatment, because then $\frac{\delta E}{\delta n(\mathbf{r})} = E_F$ is constant and because the total number of electrons $N_{\mathrm{el}} = \int \mathrm{d}\mathbf{r}\, n(\mathbf{r};\mathbf{R}^n)$ does not depend on the atomic positions. Within a full potential KKR formalism, the Kohn-Sham equations for the valence electrons are solved rather accurately, the only approximation is the $l_{\max}$ cutoff. This means that the second term usually contains a negligible contribution from the valence electrons. For the core electrons, however, this term gives a considerable contribution if the core states are calculated as usual in an atomic fashion using only the spherical part of the potential. With a spherical ansatz n_{core} for the core density, the resulting expression for the force is

$$\mathbf{F}^n = Z^n \left.\frac{\partial V_{\mathrm{M}}(\mathbf{r})}{\partial \mathbf{r}}\right|_{\mathbf{r}=\mathbf{R}^n} - \int d^3r\, n_{\mathrm{core}}(|\mathbf{r}-\mathbf{R}^n|)\, \frac{\partial v_{\mathrm{eff}}(\mathbf{r})}{\partial \mathbf{r}} \tag{30}$$

where Z^n is the nuclear charge, $V_{\mathrm{M}}(\mathbf{r})$ the Madelung potential and $v_{\mathrm{eff}}(\mathbf{r})$ the Kohn-Sham potential. Due to the vector character of the potential derivatives in (30), only the $l = 1$ components of V_{M} and v_{eff} are needed. Since these quantities are anyhow calculated in a full-potential KKR treatment, the calculation of forces is easy. There are also no Pulay corrections [34] required which arise in basis set methods if the basis functions depend on the atomic positions.

While force calculation are simple, calculations of atomic displacements, which occur if the impurity atoms are smaller or larger than the host atoms, are more complicated in the KKR method. The main reason is the site-centered angular momentum expansion used in the Green function expression (19) which is needed around the displaced sites. While original undisplaced and new displaced sites can be used together in the calculation of the Green function with appropriate artificial zero potentials on non-participating sites, it is numerically simpler to transform the Green function matrix elements from undisplaced to displaced sites [35, 36]. The reference Green function matrix elements are transformed by

$$\tilde{G}^{\mathrm{r},nn'}_{LL'}(\epsilon) = \sum_{L''L'''} U_{LL''}(\mathbf{s}^n;\epsilon) G^{\mathrm{r},nn'}_{L''L'''}(\epsilon) U_{L'L'''}(\mathbf{s}^{n'};\epsilon) \tag{31}$$

where $\mathbf{s}^n$ is the shift of atom at site $\mathbf{R}^n$ to the new site $\mathbf{R}^n + \mathbf{s}^n$. The transformation matrix is given by

$$U_{L'L}(\mathbf{s}^n;\epsilon) = 4\pi \sum_{L''} \mathrm{i}^{l'+l''-l} C_{LL'L''} j_{l''}(\sqrt{\epsilon} s^n) Y_{L''}(\hat{\mathbf{s}}^n) \tag{32}$$

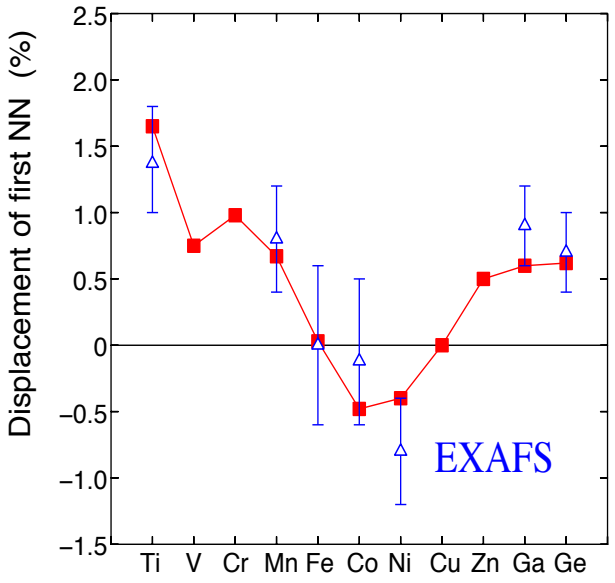

Fig. 5: *Displacements of the nearest Cu neighbors around impurities from Ti to Ge in Cu. The displacements are given in percent of the nearest neighbor distance between the atoms in unperturbed Cu. Experimental results obtained by EXAFS measurements are shown by triangles with error bars. The picture is taken from Ref. [37].*

where $C_{LL'L''} = \int_{4\pi} \mathrm{d}\hat{\mathbf{r}}\, Y_L(\hat{\mathbf{r}}) Y_{L'}(\hat{\mathbf{r}}) Y_{L''}(\hat{\mathbf{r}})$ are Gaunt coefficients, j_l spherical Bessel functions and Y_L spherical harmonics. Together with a similar transformation for the t matrix, the following algebraic Dyson equation

$$G = \tilde{G}^{\mathrm{r}} + \tilde{G}^{\mathrm{r}}[t - \tilde{t}^{\mathrm{r}}]G \tag{33}$$

must be solved. While the transformation (31) is exact, if the sums over L'' and L''' are extended over infinite angular momenta, in practical calculations these sums must be truncated. For large displacements a relatively high l_{max} value is needed, but $l_{\max} = 4$ is sufficient for displacements up to 10 % of the nearest neighbor distance as they occur around the substitutional impurities considered here.

Fig. 5 shows calculated displacements of nearest neighbor Cu atoms around impurities from the 3rd series of the periodic table together with experimental data derived from extended x-ray absorption fine structure (EXAFS) measurements. Most of the impurities lead to an outward displacement of the Cu neighbors which means that these impurities are *bigger* than Cu. Only Ni and Co are *smaller* with inward displacements. The displacements induced by Fe are very small and for a Cu impurity they are, of course, zero.

In contrast to metals, lattice relaxations in semiconductors are usually considerably larger because of more open structures and lower coordination numbers. For the defect pairs shown in Fig. 6 the displacements reach up to 10 % of the nearest neighbor distance which is about the limit for the U transformations. The figure shows a comparison of displacements calculated for donor-acceptor pairs in Si by the full-potential KKR-GF method and a pseudopotential *ab-initio* molecular dynamics program applied to a supercell with 64 atoms [38]. The displaced positions

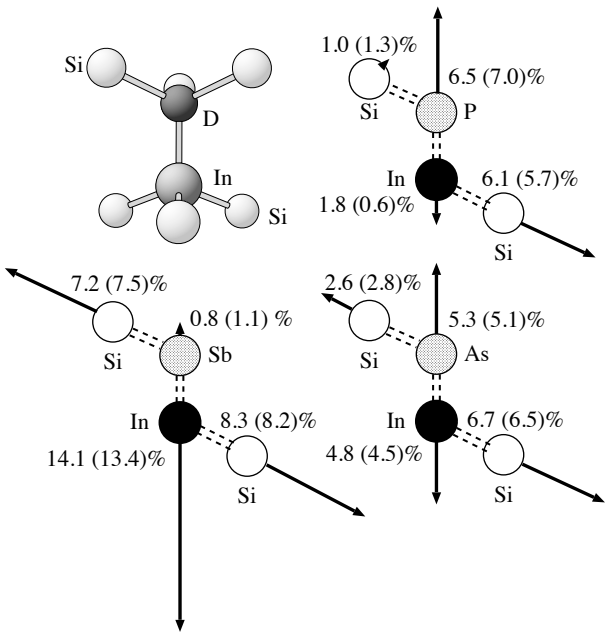

Fig. 6: *Calculated displacements for InSb, InP and InAs defect pairs in Si. The results are given in percent of the nearest neighbor distance between the bulk Si atoms. Two sets of numbers are given. The number in parentheses have been calculated by a pseudopotential method, the other number by the KKR-GF method.*

obtained by the two methods are essentially the same, but the KKR-GF method can give more information, in particular for properties that are determined by the core electrons, like hyperfine fields or electric field gradients.

The considered defect pairs are electrically and magnetically inactive and experimental information about the structure is difficult to obtain. One of the few methods to investigate such defects are perturbed angular correlation (PAC) experiments which measure the electric field gradients. The calculated electric field gradients depend sensitively on the lattice relaxations of the defect complex. While calculations without lattice relaxations give the wrong trend with respect to the atomic numbers of the donor atoms, the agreement greatly improves, if the relaxed configurations are considered [39], as for instance given in Fig. 6 for donor-acceptor pairs in Si. Thus a reliable calculation of the relaxations is crucial for understanding the electric field gradients.

Efficient and accurate force calculations open the possibility to study phonon dispersion relations. Within a Green function impurity method the calculations can be done in real space by directly determining the Born-von Karman force constants according to their definition. One atom is displaced by a finite amount and the induced forces on all atoms are calculated. Fourier transformation gives the dynamical matrix and phonon frequencies and eigenstates in the Brillouin zone are easily obtained. For cubic crystals a single self-consistent calculation is enough to determine the whole phonon spectrum. Fig. 7 shows the phonon dispersion curves of Al calculated in this way by the KKR-GF method. As can be seen a calculation including 6th near-

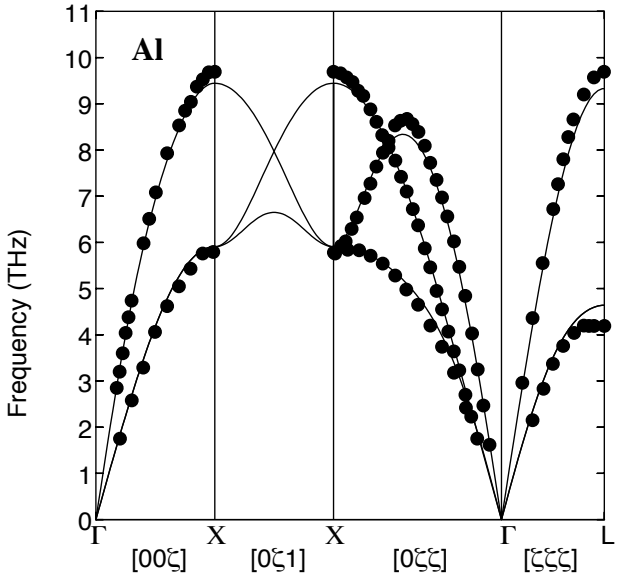

Fig. 7: *Calculated phonon spectrum (continuous lines) of fcc Al and experimental results (full dots). The central Al atom is shifted by 0.5% and the forces on six shells of neighboring atoms are calculated self-consistently, yielding force constant parameters for six nearest neighbor shells. The figure is taken from Ref. [37].*

est neighbor interactions reproduces the experimental data quite well. A disadvantage of this approach is that a relatively big cluster, including many atoms, must be used to account for long range elastic interactions present for example in semiconductors.

3.4 Long range perturbations

Magnetic impurities in non-magnetic materials induce magnetic polarization oscillations on the surrounding host atoms. Usually these oscillations are small effects. Typically a Cu atom as nearest neighbor of an impurity from the $3d$ series carries an induced moment of about $10^{-2}\mu_{\rm B}$ and the size of the moments decreases with increasing distance from the impurity as the third power of distance. Despite of this, as discussed in Ref. [40], very nice experimental information about the magnetization oscillations in Cu exists due to measurements of Knight shift satellites by the Slichter group. The measured Knight shift satellites can be related to calculated hyperfine fields as detailed in Ref. [40]. Fig. 8 shows calculated hyperfine fields on twelve shells of Cu neighbors around a Mn impurity, which means that potentials for 225 atoms have been calculated self-consistently. The corresponding experimental results derived from the Knight shift measurement are shown by red squares. Calculation and experiment nicely agree if the correct assignment of the experimentally observed peaks to the different shells has been made. While the assignment of calculated hyperfine fields to the different shells is unambiguous, the assignment of experimental peaks is more difficult. It relies on the symmetry of the shells, on the intensity of the peaks arising from the number of atoms in the shells and on the magnitude of the derived hyperfine field according to the rapid decrease with distance.

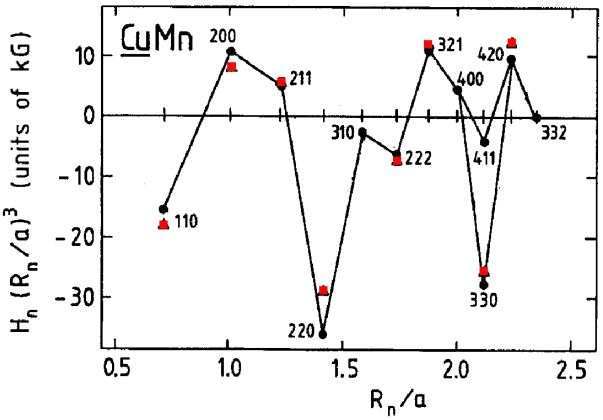

Fig. 8: *Hyperfine fields of Cu atoms in different shells around a Mn impurity in Cu. The calculated values (solid curve) were multiplied with $(R_n/a)^3$, where R_n is the distance from the Mn nucleus and a the lattice constant of Cu. The numbers indicate the different shells and the experimental values are shown as red squares. The picture is taken from Ref. [41].*

3.5 Parameters for model Hamiltonians

Green function impurity calculations can be used to obtain parameters for model Hamiltonians if constraints are applied in density functional theory [42]. Constraints are already used in the formal development of density functional theory, for instance the density is constrained to give the correct number of electrons and the Kohn-Sham orbitals must be normalized as $\sum_\alpha(\varphi_i^\alpha, \varphi_i^\alpha) = 1$. Another example is Levy's [43] explicit definition of the energy by constrained minimization over all many-electron wavefunctions which give the same density. The idea of constrained density-functional theory [42] is the extension to quite arbitrary constraints. This idea is useful if one wants to calculate total energy differences which depend on a parameter, for instance on N_V, the number of electrons inside a volume V. The constraint can be taken into account by modifying the energy functional $E[n(\mathbf{r})]$ into

$$\tilde{E}[n(\mathbf{r})] = E[n(\mathbf{r})] + v\left[N_V - \int_V n(\mathbf{r})\mathrm{d}\mathbf{r}\right] \tag{34}$$

where the constraint is guaranteed by the Lagrange parameter v. The minimization of (34) with respect to $n(\mathbf{r})$ leads to an additional potential v in the Kohn-Sham equations, which is constant and only acts in V and is zero elsewhere. This potential must be adjusted such that the resulting density $n(\mathbf{r})$ gives exactly N_V electrons in volume V. Instead of calculating the energy differences from the functional $\tilde{E}[n(\mathbf{r})]$ by subtracting the energies for different values of the parameter N_V, it is computationally easier to calculate the difference directly by the Hellmann-Feynman theorem

$$\frac{\mathrm{d}\tilde{E}(N_V)}{\mathrm{d}N_V} = v \qquad \Rightarrow \qquad \Delta\tilde{E}(N_V) = \int_{N_0}^{N_V} v(N')\,\mathrm{d}N' \tag{35}$$

which only requires the knowledge of the potential $v(N')$. Physically, the potential v can be viewed as the *force* necessary to constrain the system to the desired state and ΔE as the *strain energy* of the system.

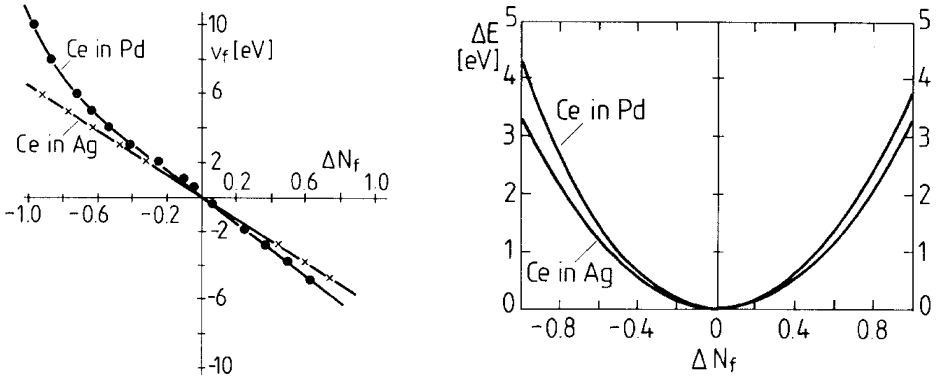

Fig. 9: *Constraining field (left) and energy difference (right) as function of the deviation of the occupation number N_f from its ground state value N_f^0. Pictures are taken from Ref. [42].*

Instead of varying the total charge it is more interesting to vary partial charges, for instance the number of d- or f-electrons in the impurity cell. Minimization then leads to a constant projection potential $v(N_{d,f})$ which acts only on states with $l = 2$ or $l = 3$ character in the considered cell. The energy differences obtained in this way can be related to the screened Coulomb parameters U_d and U_f (Hubbard *U*), for instance as

$$U_f = \Delta E(N_f^0 + 1) + \Delta E(N_f^0 - 1) \tag{36}$$

where N_f^0 is the number of f-electrons in equilibrium. In the calculation the screening is provided by the the s- and p-states which can adjust to the changed number of d- or f-electrons.
An early application of constrained density functional theory was the calculation of the Coulomb parameter U_f for Ce impurities in Ag and Pd [42]. The number N_f of f-electrons was determined by integrating the local density of states (12) using only $l = 3$ angular momentum components for $n(\epsilon)$. The ground state values of N_f were determined as $N_f^0 = 1.18$ for Ce in Pd and as $N_f^0 = 1.25$ for Ce in Ag. A constraining projection potential v_f was applied within the muffin-tin sphere around the Ce impurity and the dependence of N_f on v_f was determined. Both the constraining potential and the energy difference are plotted in Fig. 9. The dependence of v_f on N_f is almost linear except for Pd near $\Delta N_f = -1$, where it becomes increasingly difficult to remove all f-states due to their strong hybridization with d-states of Pd. The energy differences depend almost quadratically on ΔN_f and the screened Coulomb parameters according to (36) turned out be 6.6 eV for Ce in Ag and 8.1 eV in Pd.
Another early application of constrained density functional theory was the calculation of interaction energy differences between the ferromagnetic and antiferromagnetic configuration of impurity pairs in metals [44]. In these calculations the local magnetic moment of one of the impurities is constrained to an arbitrary value M and the lowest energy compatible with the constraint is determined by a modified functional

$$\tilde{E}[n(\mathbf{r}), m(\mathbf{r})] = E[n(\mathbf{r}), m(\mathbf{r})] + H\left[M - \int_V m(\mathbf{r})\mathrm{d}\mathbf{r}\right]$$

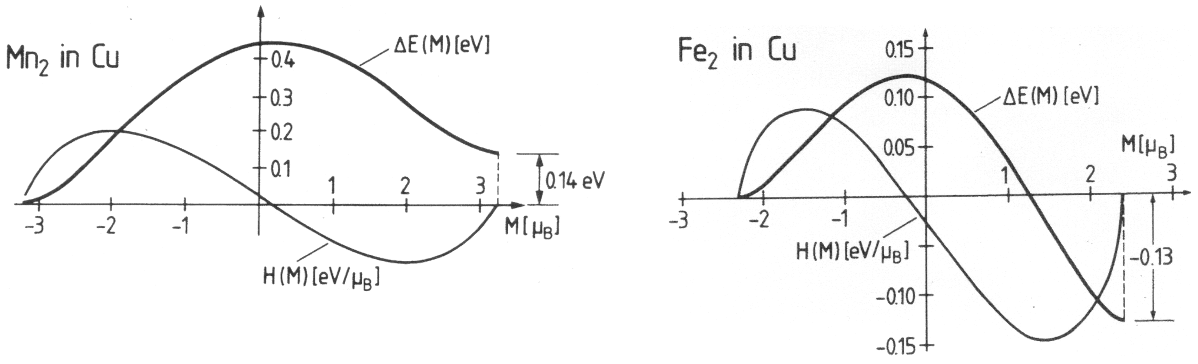

Fig. 10: *Difference of the magnetic interaction energy difference $\Delta E(M)$ and the constraining magnetic field $H(M)$ as function of the prescribed local impurity moment. The results are for pairs of Mn and Fe impurities on nearest neighbor sites in a Cu crystal (from Ref. [44]).*

where the Lagrange parameter H is a constraining longitudinal magnetic field, which is constant in the cell of one impurity with volume V and zero elsewhere. This field is chosen such that the integral of the magnetization $m(\mathbf{r})$ over the cell gives the desired value of the moment.
Similar to (35) the energy difference is given by

$$\Delta E(M) = \int_{M_0}^{M} H(M')\mathrm{d}M'$$

where M_0 is the value of M in the reference state. For instance in Fig. 10, the reference state is the antiferromagnetic configuration, for which the moments for the two impurities have opposite sign. This state corresponds to the left minima of the $\Delta E(M)$ curves in Fig. 10, while the right minima correspond to the ferromagnetic configuration. Both configurations are stable as the energy minima with vanishing constraining field H indicate. The energy differences between different magnetic configurations determine exchange parameters J_{ij} which may be used in a Heisenberg model

$$\hat{H} = -\sum_{i,j} J_{ij}\underline{\hat{S}}_i\underline{\hat{S}}_j \,,$$

which can be treated much faster for large and complex systems than fully self-consistent spin density functional calculations.

4 Random Alloys and CPA

For real alloys the consideration of one or even two impurities is relevant only for the very dilute limit where interactions between impurity clusters can safely be neglected. For increasing impurity concentration these interactions become more and more important. Instead of calculating the Green function for a single configuration realized in a particular system, one is then interested in spatial or configurational averages $\langle G\rangle$ of the Green function over many different possible configurations [45]. For the derivation of expressions for the averaged Green function

$\langle G\rangle$ it is convenient to consider first the single-site problem and then the interaction between the different sites. The single-site problem can be written in operator notation as

$$G_\alpha = g + gV_\alpha G_\alpha \tag{37}$$

where all quantities are considered as integral operators[3] and g and V_α are used as shorter notations for G^{r} and Δv^n. In order to emphasize that in this section single-site quantities are integral operators, the sites are labelled here by Greek letters. With the definition $t_\alpha g = V_\alpha G_\alpha$ the last equation can be solved as

$$G_\alpha = g + gt_\alpha g\ . \tag{38}$$

Multiplication with V_α from the left leads to

$$V_\alpha G_\alpha = t_\alpha g = V_\alpha g + V_\alpha g t_\alpha g\ . \tag{39}$$

This is valid if t_α is determined by

$$t_\alpha = V_\alpha + V_\alpha g t_\alpha\ . \tag{40}$$

Using spatial variables the last equation can be written as

$$t_\alpha(\mathbf{r},\mathbf{r}') = V_\alpha(\mathbf{r})\delta(\mathbf{r}-\mathbf{r}') + \int \mathrm{d}\mathbf{r}''\, V_\alpha(\mathbf{r}) g(\mathbf{r},\mathbf{r}'') t_\alpha(\mathbf{r}'',\mathbf{r}') \tag{41}$$

where the potential operator is local as characterized by the delta function. By iterating (40) as $t_\alpha = V_\alpha + V_\alpha g V_\alpha + V_\alpha g V_\alpha g V_\alpha \ldots$ one sees that t_α is a single-site quantity. It is only needed in cell α because all terms contain factors V_α on the left and right and V_α is restricted to cell α.
For the multiple-site problem, where the potential perturbation is given by $V = \sum_\alpha V_\alpha$, it is convenient to introduce an operator F which connects G and its average $\langle G\rangle$ by

$$G = F\langle G\rangle\ . \tag{42}$$

If this is used in $G = g + gVG$, which is (14) in operator notation, the result is

$$F\langle G\rangle = g + gVF\langle G\rangle \tag{43}$$

Averaging gives

$$\langle G\rangle = g + g\langle VF\rangle\langle G\rangle \tag{44}$$

where $\langle F\rangle = 1$ was used which follows from (42). The last equation contains only averaged quantities and could be solved easily if $\langle VF\rangle$ is known.[4]
The task is now to derive an equation for $\langle VF\rangle$. Subtraction of (43) and (44) and omitting the common operator $\langle G\rangle$ on both sides of the resulting equation gives

$$F - 1 = g(VF - \langle VF\rangle)\ . \tag{45}$$

[3] Integral operators, for instance g, act on arbitrary functions $f(\mathbf{r})$ as $\int \mathrm{d}\mathbf{r}' g(\mathbf{r},\mathbf{r}') f(\mathbf{r}')$.
[4] The quantity $\langle VF\rangle$ is usually called self-energy and labelled by the letter Σ.

which multiplied with V leads to

$$VF = V + Vg(VF - \langle VF \rangle) \tag{46}$$

This is the basic result used for further considerations. Now the crucial point is that VF can be written as a sum of single-site terms. For that purpose operators f_α are defined by the equation $V_\alpha F = t_\alpha f_\alpha$. With $V = \sum_\alpha V_\alpha$ one obtains $VF = \sum_\alpha V_\alpha F = \sum_\alpha t_\alpha f_\alpha$ and (46) can be written as

$$\sum_\alpha t_\alpha f_\alpha = \sum_\alpha V_\alpha + \sum_\alpha \sum_\beta V_\alpha g t_\beta f_\beta - \sum_\alpha \sum_\beta V_\alpha g \langle t_\beta f_\beta \rangle \; . \tag{47}$$

On the other hand, if (40) is multiplied with f_α and summed over α, the result is

$$\sum_\alpha t_\alpha f_\alpha = \sum_\alpha V_\alpha f_\alpha + \sum_\alpha V_\alpha g t_\alpha f_\alpha \; . \tag{48}$$

Subtraction of (47) and (48) gives

$$0 = \sum_\alpha V_\alpha (f_\alpha - 1 - \sum_{\beta \neq \alpha} g t_\beta f_\beta + \sum_\beta g \langle t_\beta f_\beta \rangle) \tag{49}$$

where the restriction $\beta \neq \alpha$ arises from the subtraction of the last term of (48). The last equation is satisfied if f_α is determined by the implicit equation

$$f_\alpha = 1 + \sum_{\beta \neq \alpha} g t_\beta f_\beta - \sum_\beta g \langle t_\beta f_\beta \rangle \; . \tag{50}$$

In general, this equation cannot be solved exactly, but it can be used to obtain approximations. Iteration of (50) starting with $f_\alpha = 0$ leads to

$$\begin{aligned} f_\alpha = {} & 1 \\ & + \sum_{\beta \neq \alpha} g t_\beta - \sum_\beta g \langle t_\beta \rangle \\ & + \sum_{\beta \neq \alpha} \sum_{\gamma \neq \beta} g t_\beta g t_\gamma - \sum_{\beta \neq \alpha} \sum_\gamma g t_\beta g \langle t_\gamma \rangle - \sum_\beta \sum_{\gamma \neq \beta} g \langle t_\beta g t_\gamma \rangle + \sum_\beta \sum_\gamma g \langle t_\beta \rangle g \langle t_\gamma \rangle \\ & + \ldots \end{aligned} \tag{51}$$

where terms containing three or more t operators are not shown. In order to obtain approximations for $\langle VF \rangle$ the last equation is multiplied with t_α, summed over α and averaged. This leads to

$$\begin{aligned} \langle VF \rangle = {} & \sum_\alpha \langle t_\alpha \rangle \\ & + \sum_\alpha \sum_{\beta \neq \alpha} \langle t_\alpha g t_\beta \rangle - \sum_\alpha \sum_\beta \langle t_\alpha \rangle g \langle t_\beta \rangle \\ & + \sum_\alpha \sum_{\beta \neq \alpha} \sum_{\gamma \neq \beta} \langle t_\alpha g t_\beta g t_\gamma \rangle - \sum_\alpha \sum_{\beta \neq \alpha} \sum_\gamma \langle t_\alpha g t_\beta \rangle g \langle t_\gamma \rangle \\ & - \sum_\alpha \sum_\beta \sum_{\gamma \neq \beta} \langle t_\alpha \rangle g \langle t_\beta g t_\gamma \rangle + \sum_\alpha \sum_\beta \sum_\gamma \langle t_\alpha \rangle g \langle t_\beta \rangle g \langle t_\gamma \rangle + \ldots \; . \end{aligned} \tag{52}$$

Here it is important to note that this expression is still exact although only terms up to third order in t_α are written down.
Now approximations can be made. An important approximation, which leads to a considerable simplification, is the neglect of correlations between different sites. While electronic structure calculations for alloys nowadays do not necessarily need this approximation, for instance in the non-local CPA of Rowlands *et al.* [46, 47], these advanced techniques are difficult to discuss and will not be considered here. The neglect of correlations means that averages $\langle t_\alpha g t_\beta \rangle$ can be factorized as $\langle t_\alpha \rangle \langle t_\beta \rangle$ if the sites α and β are different. This leads to

$$\begin{aligned} \langle VF \rangle = & \sum_\alpha \langle t_\alpha \rangle - \sum_\alpha \langle t_\alpha \rangle g \langle t_\alpha \rangle \\ & + \sum_\alpha \langle t_\alpha \rangle g \langle t_\alpha \rangle g \langle t_\alpha \rangle + \sum_\alpha \sum_{\beta \neq \alpha} \langle t_\alpha g \langle t_\beta \rangle g t_\alpha \rangle - \sum_\alpha \sum_{\beta \neq \alpha} \langle t_\alpha \rangle g \langle t_\beta \rangle g \langle t_\alpha \rangle - \dots . \end{aligned} \tag{53}$$

From this expression a number of approximations can be derived which are far better than the most simple approximation which replaces $\langle VF \rangle$ by $\langle V \rangle = \sum_\alpha \langle V_\alpha \rangle$. This approximation which only uses the averaged potential is called the virtual crystal approximation (VCA). It is easy to handle because it leads to a real potential, but has serious deficits for describing real disordered systems. A major improvement on the VCA is to use the first term of (53) or (52). This approximation is called average t matrix approximation (ATA) and takes into account all effects up to first order in the t operator. The ATA has been extensively discussed in the literature, in particular in connection with multiple-scattering theory [48, 49]. A simple way to go beyond the ATA is to use all terms of (53) which contain only a single site α. The result can written as $\sum_\alpha (1 + g\langle t_\alpha \rangle)^{-1} \langle t_\alpha \rangle$ and corresponds to the optical potential discussed by Goldberger and Watson [51]. This method is correct to second order in the t operator, the third order terms not treated are the last two ones shown in (53). An even better approximation is obtained by realizing that the above equations are valid for quite arbitrary Green functions g provided that the corresponding reference system shows no disorder. In a self-consistent procedure the reference Green function g is chosen in such a way that as many terms as possible vanish in (53). In principle, one could demand $\langle t_\alpha(\mathbf{r}, \mathbf{r}') \rangle = 0$. In general this is, however, not possible because the integral operator $t_\alpha(\mathbf{r}, \mathbf{r}')$ is a complicated function of $\mathbf{r}$ and $\mathbf{r}'$. In the multiple-scattering KKR method the situation is somewhat simpler because it relies on algebraic matrices t^n instead of integral operators t_α. Then, as shown by Soven [50] self-consistency can be implemented by choosing an effective reference medium with the requirement that the scattering of the electrons averaged over the constituent atoms vanishes in the effective medium. The resulting approximation called KKR-CPA has been widely applied to study the electronic structure of disordered alloys.
As an example for extensive KKR-CPA calculations Fig. 11 shows results [52] for the averaged local magnetic moments in alloys of Fe, Co, and Ni and alloys of these elements with other transition metals. The diagrams obtained on the left for the experimental results and on the right for the calculated results are referred to as Slater-Pauling curves. The Slater-Pauling curve has two main branches with slopes of 45^o and -45^o which meet in the middle where a maximal

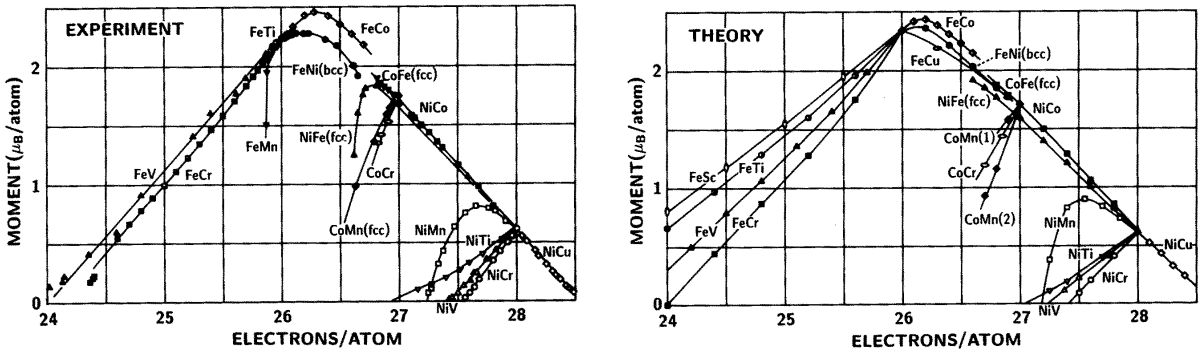

Fig. 11: *Slater-Pauling curve for the averaged magnetic moment per atom as function of the averaged number of electrons per atom. The picture is taken from Ref. [52].*

moment of about 2.4 μ_{B} occurs. The left main branch consists of Fe alloys, whereas Co and Ni alloys form the right main branch and the subbranches. The main reason for the two different slopes is a different electronic screening behavior. Alloys on the main branch on the right have a full majority spin band so that the screening of the valence difference introduced by the impurity atoms is provided by minority spin electrons. This leads to a reduced number of minority d-electrons which gives increased moments. Alloys on the other branches are characterized by the occurrence of antiparallel moments of the impurities which lead to reduced averaged moments with increasing concentration. Here the screening is mainly provided by the majority spin electrons. Although the agreement between experiment and calculation is not perfect, Fig. 11 shows that spin density functional theory is a powerful tool to understand and explain magnetic properties of materials.

Appendix

A Useful Green function properties

The Green function $G(\epsilon)$ for a Hamiltonian $\mathcal{H}$ is defined by the operator equation

$$G = \frac{1}{\epsilon - \mathcal{H}} \,. \tag{54}$$

For real ϵ it is necessary to perform a limiting process. Then the real quantity ϵ is replaced by a complex quantity $\epsilon + i\gamma$ and all equations are understood in the sense that the limit $\gamma \to 0+$ must be performed in the end. The relation

$$\lim_{\gamma \to 0+} \frac{1}{\epsilon + i\gamma - \mathcal{H}} = P\frac{1}{\epsilon - \mathcal{H}} - i\pi\delta(\epsilon - \mathcal{H}) \tag{55}$$

where P denotes the principal value, establishes the connection between the imaginary part of the Green function and the density of states $n(\epsilon) = \delta(\epsilon - \mathcal{H})$ and also the Kramers-Kronig relation between the imaginary and the real part of the Green function

$$\operatorname{Im} G(\epsilon) = -\pi n(\epsilon) \,, \qquad \operatorname{Re} G(\epsilon) = -\frac{1}{\pi} P \int_{-\infty}^{\infty} \frac{1}{\epsilon - \epsilon'} \operatorname{Im} G(\epsilon') \, \mathrm{d}\epsilon' \,. \tag{56}$$

where the last equation is a Hilbert transform.
While the above equations in this appendix are valid for real values of ϵ, complex values of ϵ are considered below. Then the last equation can be generalized to

$$G(\epsilon) = -\frac{1}{\pi} \int_{-\infty}^{\infty} \frac{1}{\epsilon - \epsilon'} \operatorname{Im} G(\epsilon') \, \mathrm{d}\epsilon' \,. \tag{57}$$

Another useful relation for the Green function is given by

$$\frac{\mathrm{d}G(\epsilon)}{\mathrm{d}\epsilon} = \frac{\mathrm{d}}{\mathrm{d}\epsilon} \frac{1}{\epsilon - \mathcal{H}} = -\frac{1}{\epsilon - \mathcal{H}} \frac{1}{\epsilon - \mathcal{H}} = -G(\epsilon)\, G(\epsilon) \,. \tag{58}$$

The electronic density of states can formally be expressed as

$$n(\epsilon) = -\frac{1}{\pi} \operatorname{Im} \operatorname{Tr} G\,(\epsilon) \,. \tag{59}$$

The difference between the density of states for two systems characterized by two Green-function operators $G(\epsilon)$ and $g(\epsilon)$ is given by

$$\Delta n(\epsilon) = -\frac{1}{\pi} \operatorname{Im} \operatorname{Tr}[G(\epsilon) - g(\epsilon)] = -\frac{1}{\pi} \operatorname{Im} \operatorname{Tr}[g(\epsilon) V G(\epsilon)] = -\frac{1}{\pi} \operatorname{Im} \operatorname{Tr} \left[g(\epsilon) V \frac{1}{1 - g(\epsilon) V} g(\epsilon) \right] .$$

Here and below V denotes the difference between the two potentials. By use of (58) for $g(\epsilon)$ this can be expressed as

$$\Delta n(\epsilon) = \frac{1}{\pi} \operatorname{Im} \operatorname{Tr} \left[\frac{\mathrm{d}g(\epsilon)}{\mathrm{d}\epsilon} V \frac{1}{1 - g(\epsilon) V} \right] = -\frac{1}{\pi} \operatorname{Im} \operatorname{Tr} \frac{\mathrm{d}}{\mathrm{d}\epsilon} \ln(1 - g(\epsilon) V) \,. \tag{60}$$

The difference between the integrated densities of states is thus given by

$$\Delta N(\epsilon) = \int^{\epsilon} d\epsilon' \, \Delta n(\epsilon') = -\frac{1}{\pi} \operatorname{Im} \operatorname{Tr} \ln(1 - g(\epsilon) V) \tag{61}$$

References

[1] J. Korringa 1947 Physica **13**, 392 (1947)

[2] W. Kohn and N. Rostoker, Phys. Rev. **94**, 1111 (1954)

[3] P. Hohenberg and W. Kohn, Phys. Rev. **136**, B864 (1964)

[4] W. Kohn and L.J. Sham, Phys. Rev. **140**, A1133 (1965)

[5] E.N. Economou: *Green's Functions in Quantum Physics* (Springer, Berlin, 2011)

[6] C. Koenig, J. Phys. F: Metal Phys. **3**, 1497 (1973)

[7] H. Dreysse and R. Riedinger, J. Physique **42**, 437 (1981)

[8] R. Zeller, J. Deutz and P.H. Dederichs, Solid State Commun. **44**, 993 (1982)

[9] A.R. Williams, P.J. Feibelman and N.D. Lang, Phys. Rev. B **26**, 5433 (1982)

[10] G.F. Koster and J.C. Slater, Phys. Rev. **94**, 1392 (1954); Phys. Rev. **95**, 1164 (1954)

[11] G.A. Baraff and M. Schlüter, Phys. Rev. Lett. **41**, 892 (1978)

[12] J. Bernholc, N.O. Lipari and S.T. Pantelides, Phys. Rev. Lett. **41**, 895 (1978)

[13] S.P. Singhal and J. Callaway, Phys. Rev. B **19**, 5049 (1979)

[14] C. Koenig and E. Daniel, J. Phys. (Paris) **42**, L193 (1981)

[15] O. Gunnarsson, O. Jepsen and O.K. Andersen, Phys. Rev. B **27**, 7144 (1983)

[16] R. Zeller and P.H. Dederichs, Phys. Rev. Lett. **42**, 1713 (1979)

[17] R. Podloucky, R. Zeller and P.H. Dederichs, Phys. Rev. B **22**, 5777 (1980)

[18] R. Zeller and P.J. Braspenning, Solid State Commun. **42**, 701 (1982)

[19] G.M. Stocks, W.M. Temmerman and B.L. Gyorffy, Phys. Rev. Lett. **41**, 339 (1978)

[20] A. Bansil, Phys. Rev. Lett. **41**, 1670 (1978)

[21] R. Zeller, J. Phys. C: Solid State Phys. **20**, 2347 (1987)

[22] P. Lloyd, Proc. Phys. Soc. London **90**, 207 (1967)

[23] R. Zeller, J. Phys. Condens. Matter **16**, 6453 (2004)

[24] P.W. Anderson, Phys. Rev. **124**, 41 (1961)

[25] R. Zeller, R. Podloucky and P.H. Dederichs, Z. Phys. **38**, 165 (1980)

[26] K.H. Johnson, D.D. Vvedensky and R.P. Messmer, Phys. Rev. B **19**, 1519 (1979)

[27] P.J. Braspenning, R. Zeller, A. Lodder and P.H. Dederichs, Phys. Rev. B **29**, 703 (1984)

[28] D. van der Marel, G.A. Sawatzky and F.U. Hillebrecht, Phys. Rev. Lett. **41**, 206 (1984)

[29] D. van der Marel, C. Westra, G.A. Sawatzky and F.U. Hillebrecht, Phys. Rev. B **31**, 1936 (1985)

[30] M.J. Puska, S. Pöykkö, M. Pesola and R.M. Nieminen, Phys. Rev. B **58**, 1318 (1998)

[31] F. Corsetti and A.A. Mostofi, Phys. Rev. B **84**, 035209 (2011)

[32] P.H. Dederichs, B. Drittler and R. Zeller, in: *Applications of Multiple Scattering Theory to Materials Science*, ed. by W.H. Butler, P.H. Dederichs, A. Gonis and R. Weaver, MRS Symposia Proceedings No. 253, (Materials Research Society, Pittsburgh, 1992)

[33] B. Drittler, M. Weinert, R. Zeller and P.H. Dederichs, Solid State Commun. **79**, 31 (1991)

[34] P. Pulay, Mol. Phys. **17**, 153 (1969)

[35] N. Stefanou, P.J. Braspenning, R. Zeller and P.H. Dederichs, Phys. Rev. B **36**, 6372 (1987)

[36] N. Papanikolaou, R. Zeller, P.H. Dederichs and N. Stefanou, Phys. Rev. B **55**, 4157 (1997)

[37] N. Papanikolaou, R. Zeller and P.H. Dederichs, J. Phys Condens. Matter **14**, 2799 (2002)

[38] A. Settels, K. Schroeder, T. Korhonen, N. Papanikolaou, M. Aretz, R. Zeller and P.H. Dederichs, Solid State Commun. **113**, 239 (2000)

[39] A. Settels, T. Korhonen, N. Papanikolaou, R. Zeller and P.H. Dederichs, Phys. Rev. Lett **83**, 4369 (1999)

[40] B. Drittler, H. Ebert, R. Zeller and P.H. Dederichs, Phys. Rev. B **39**, 6334 (1989)

[41] P.H Dederichs, P. Lang, K. Willenborg, R. Zeller, N. Papanikolaou and N. Stefanou, Hyperfine Interact. **78**, 341 (1993)

[42] P.H. Dederichs, S. Blügel, R. Zeller and H. Akai, Phys. Rev. Lett **53**, 2512 (1984)

[43] M. Levy, Proc. Natl. Acad. Sci. U.S.A. **76**, 6062 (1979)

[44] A. Oswald, R. Zeller and P.H. Dederichs, J. Magn. Magn. Mater. **140-144**, 1247 (1986)

[45] R.J. Elliot, J.A. Krumhansl and P.L. Leath, Rev. Mod. Phys. **46**, 465 (1974)

[46] D.A. Rowlands, J.B. Staunton, B.L. Györffy, E. Bruno and B. Ginatempo, Phys. Rev. B **72**, 045101 (2005)

[47] D.A. Rowlands, Rep. Prog. Phys. **72**, 086501 (2009)

[48] J. Korringa, J. Phys. Chem. Solids **7**, 252 (1958)

[49] J.L. Beeby and S.F. Edwards, Proc. R. Soc. (Lond.) A **274**, 395 (1963)

[50] P. Soven, Phys. Rev. **156**, 809 (1967)

[51] M.L. Goldberger and K.M. Watson, *Collision Theory* (Wiley, New York, 1964)

[52] P.H. Dederichs, R. Zeller, H. Akai and H. Ebert, J. Magn. Magn. Mater. **100**, 241 (1991)